

# Angular Momentum about the Contact Point for Control of Bipedal Locomotion: Validation in a LIP-based Controller

Yukai Gong and Jessy Grizzle

**Abstract**—In the control of bipedal locomotion, linear velocity of the center of mass has been widely accepted as a primary variable for summarizing a robot’s state vector. The ubiquitous massless-legged linear inverted pendulum (LIP) model is based on it. In this paper, we argue that angular momentum about the contact point has several properties that make it superior to linear velocity for feedback control. So as not to confuse the benefits of angular momentum with any other control design decisions, we first reformulate the standard LIP controller in terms of angular momentum. We then implement the resulting feedback controller on the 20 degree-of-freedom bipedal robot, Cassie Blue, where each leg accounts for nearly one-third of the robot’s total mass of 35 Kg. Under this controller, the robot achieves fast walking, rapid turning while walking, large disturbance rejection, and locomotion on rough terrain. The reasoning developed in the paper is applicable to other control design philosophies, whether they be Hybrid Zero Dynamics or Reinforcement Learning.

## I. INTRODUCTION

One of the core problems in the design of feedback controllers for bipedal robots is how to manage the tradeoff between the desire to achieve highly dynamic, agile behaviors, while at the same time overcoming the theoretical and practical obstructions imposed by high-dimensional dynamics (dimension 30 or more) associated with modern robots. The more dynamic and agile the behavior, the closer one must work to the limits of the machine’s capability, and hence the more crucial it is to account for the full dynamics of the robot.

Control engineers have confronted an analogous problem for over a century: a robust high-bandwidth closed-loop system requires good knowledge of the open-loop model, while for a low-bandwidth closed-loop system, it is sometimes enough to only know the sign of the DC gain. Taking the analogy between agility and closed-loop bandwidth one step further, control engineers also know that it matters what the control variable is. For example, in a single-input single-output control system, the zeros of the transfer function limit the bandwidth of a well-designed closed-loop system [7].

The major theme of this paper is that in the feedback control of bipedal locomotion, the choice of primary control variable is also very important. Here, we will first argue and then

demonstrate in experiments that a biped’s angular momentum about the contact point has multiple properties that make it a better variable for feedback control than is linear velocity or linear momentum. So as not to confuse the benefits of angular momentum with any other control design decisions, we chose to demonstrate our results by reformulating the well-known linear Inverted Pendulum (LIP) controller [19] in terms of angular momentum. Because every student of bipedal locomotion control is familiar with the LIP controller, we feel that this gives us the best chance of transferring our ideas to the bipedal community with a maximum of transparency.

Of course, the LIP model is a greatly simplified representation of a bipedal robot. One of its key assumptions is that the legs of the robot are massless. To demonstrate that our results transfer in practice to a realistic bipedal robot, we implement the resulting feedback controller on the 20 degree-of-freedom bipedal robot, Cassie Blue, where each leg accounts for nearly one-third of the robot’s total mass of 35 Kg. Moreover, the implementation is purposely done without any optimization so as to aid other groups in the transfer of our results to their robots. In experiments, Cassie Blue is able to execute walking in a straight line up to 2.1 m/s, simultaneously walking forward and diagonally on grass at 1 m/s, make quick, sharp turns, and handle very challenging undulating terrain.

The main contributions of the paper are as follows:

- Delineate desirable properties of angular momentum;
- Reformulate the LIP-based control strategy in terms of angular momentum so as to separate the benefits of angular momentum from any other control design decision. This is done because there are literally thousands of papers using LIP.
- Demonstrate the resulting controller on a very dynamic 3D bipedal robot with legs that are far from massless.
- Implement the controller in such a way that other groups can easily transfer it to their control formulation.

## A. Literature Review

The Zero-Moment Point (ZMP) is a standard control methodology in 3D humanoid robots [5], [17], [18], [20]. Because the method requires a non-zero support polygon, many robots that use it have been equipped with large feet [28]. A search on Google Scholar for papers that includes “ZMP” and “Robot” reveals 13,700 publications. Controllers based on various pendulum models are also very wide spread [3], [6], [19], [22], [24], [27]. A search on “Spring Loaded

Funding for this work was provided in part by the Toyota Research Institute (TRI) under award number No. 02281 and in part by NSF Award No. 1808051. All opinions are those of the authors.

The authors are with the College of Engineering and the Robotics Institute, University of Michigan, Ann Arbor, MI 48109 USA {ykgong, grizzle}@umich.edu

Inverted Pendulum’, and “Robot” reveals 1,760 publications; “Linear Inverted Pendulum” and “Robot” garners 3,370 publications. These methods all seek to replace the complexity of a bipedal robot with a low-dimensional model. How to “lift” the ZMP- and Pendulum-inspired control schemes from the low-dimensional representation to the full robot without “detuning” the controller (i.e., lowering its agility) is always a challenge.

The method of virtual constraints and hybrid zero dynamics (HZD) was invented so that the control design could be performed directly on the full-order dynamic model [12], [30]. It has since been expanded by many authors [10], [16], [21], [25] Virtual constraints and HZD have provided a more direct path for passing from design to implementation in terms of achievable performance. A Google Scholar search on “Hybrid Zero Dynamics” and “Robot” turns up 1,580 publications.

The current paper will focus on the original LIP formulation in [19] for the primary controller design. As we explained previously, this decision was made to enhance the ability of other groups to transfer our results to their controller design methodology. When we move to implementing our proposed control on Cassie Blue, we will use virtual constraints *in a very approximate manner* so that the closed-loop system will satisfy the key assumptions of a LIP model. By “approximate manner”, we mean that we will purposely avoid optimization of the virtual constraints; instead, they will be hand designed.

## B. Robot Testbeds

We will use both Rabbit [4] and Cassie Blue to illustrate our developments in the paper. Experiments will be conducted exclusively on Cassie. Rabbit is 2D biped with five links, four actuated joints, and a mass of mass of 32 Kg; see Fig. 2. Each leg weighs 10 kg, with 6.8 kg on thigh and 3.2 kg on shin.

The bipedal robot shown in Fig. 1, named Cassie Blue, is designed and built by Agility Robotics. The robot weighs 32kg. It has 7 deg of freedom on each leg, 5 of which are actuated by motors and 2 are constrained by springs; see Fig. 3. A floating base model of Cassie has 20 degrees of freedom. Each foot of the robot is blade-shaped and provides 5 holonomic constraints when it is on ground. Though each of Cassie’s legs has approximately 10 kg of mass, most of the mass is concentrated on the upper part of the leg. In this regard, the mass distribution of Rabbit is a bit more typical of bipedal robots, which is why we include the Rabbit model in the paper.

The remainder of the paper is organized as follows. Section II and III introduce angular momentum and the LIP model. In Section IV, we show how to predict the evolution of angular momentum with a LIP model and how to use the prediction to decide foot placement. This provides a feedback controller that will stabilize a 3D LIP. In Section V, we provide our path to implementing the controller on Cassie Blue. Additional reference trajectories are required beyond a path for the swing foot, and we provide “an intuitive” method for their design. Section VI addresses several practical challenges associated with the passage from simulation to

experimental implementation on Cassie. Section VII shows the experiment results. Conclusion are give in Sect. VIII.

## II. ANGULAR MOMENTUM ABOUT CONTACT POINT

Some of the properties of angular momentum in bipedal locomotion have been discussed in [13], [23], [30], and in [11], non-holonomic virtual constraints are created with angular momentum. The view we take here is considerably different for these references. In the following, we will address two questions: why we can replace linear momentum with angular momentum for the design of feedback controllers and what are the benefits of doing so.

Initially, we address the *single support* phase of walking, meaning only one leg is in contact with the ground. Moreover, we are considering a point contact.

Let  $L$  denote the **angular momentum** about the contact point of the stance leg. The relationship between angular momentum and **linear momentum** for a 3D bipedal robot is

$$L = L_{\text{CoM}} + p \times m_{\text{tot}} v_{\text{CoM}}, \quad (1)$$

where  $L_{\text{CoM}}$  is the angular momentum about the center of mass,  $v_{\text{CoM}}$  is the linear velocity of the center of mass,  $m_{\text{tot}}$  is the total mass of the robot, and  $p$  is the vector emanating from the contact point to the center of mass.

For a bipedal robot that is walking instead of doing somersaults, the angular momentum about the center of mass must oscillate about zero. Hence, (1) implies that the difference between  $L$  and  $p \times m v_{\text{CoM}}$  also oscillates around zero, which we will write as

$$L - p \times m_{\text{tot}} v_{\text{CoM}} = L_{\text{CoM}} \text{ oscillates about } 0. \quad (2)$$

From (2), we see that we approximately obtain a desired linear velocity by regulating  $L$ .

The discussion so far has focused on a single support phase of a walking gait. Bipedal walking is characterized by the transition between left and right legs as they alternately take on the role of stance leg (aka support leg) and swing leg



Fig. 1: Cassie Blue, by Agility Robotics, on the iconic University of Michigan Wave Field.

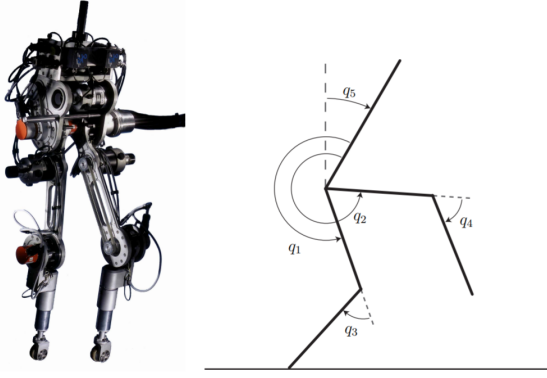


Fig. 2: Rabbit is an underactuated planar bipedal robot with point feet. Its floating base model has seven degrees of freedom and four actuators.

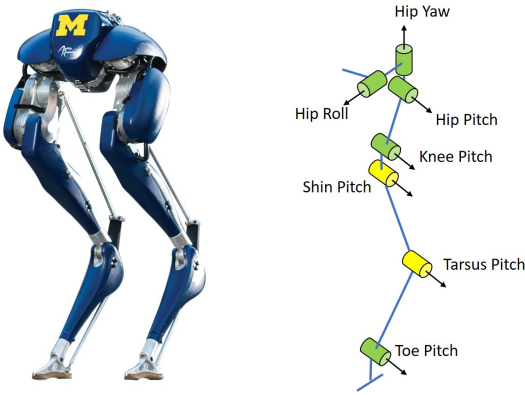


Fig. 3: Cassie bipedal robot along with the kinematics of one leg. The five green joints are actuated and two yellow joints are constrained by very rigid springs. When springs deflections are 0. Shin Pitch angle is 0 and Tarsus Pitch angle is negative Knee Pitch angle plus a 13 degree offset. Notice: In following text, toe refer to the position of toe joint.

(aka non-stance leg). In double support, the transfer of angular momentum between the two contact points satisfies

$$L_2 = L_1 + p_{2 \rightarrow 1} \times m_{\text{tot}} v_{\text{CoM}} \quad (3)$$

where  $L_i$  is the angular momentum about contact point  $i$  and  $p_{1 \rightarrow 2}$  is the vector from contact point 1 to contact point 2.

Hence, one can replace the control of linear velocity with control of angular momentum about the contact point. **But what are the advantages?**

- (a) The first advantage of controlling  $L$  is that it provides a more comprehensive representation of current walking status by including both  $L_{\text{CoM}}$  and  $p \times m v_{\text{CoM}}$ , between which momentum moves forth and back during a step.
- (b) Secondly,  $L$  has a relative degree three with respect to motor torques, if ankle torque is zero. Indeed, in this case,

$$\dot{L} = p \times m_{\text{tot}} g. \quad (4)$$

where  $g$  is the gravitational constant. Consequently,  $L$  is very weakly affected by peaks in motor torque that often occur in off nominal conditions. Moreover, if a limb, such as the swing leg, is moving quickly in response to a disturbance, it will strongly affect the angular momentum about the center of mass and the robot's linear velocity, while leaving the angular momentum about the contact point only weakly affected.

- (c) Thirdly,  $\dot{L}$  is ONLY a function of the center of mass position, making it easy to predict its trajectory over a step.
- (d) Angular momentum about a given contact point is invariant under impacts at that point, and the change of angular momentum between two contact points depends only on the vector defined by the two contact points and the CoM velocity. Hence, we can easily determine the angular momentum about the new contact point by (3) when impact happens without approximating assumptions about the impact model. Moreover, if the vertical component of the  $v_{\text{CoM}}$  is zero and the ground is level, then  $p_{2 \rightarrow 1} \times m_{\text{tot}} v_{\text{CoM}} = 0$  and hence  $L_2 = L_1$ .

Figure 4 shows simulation plots of  $L$ ,  $L_{\text{CoM}}$ , and  $v_{\text{CoM}}^x$  for the planar bipedal robot, Rabbit, and the 3D bipedal robot, Cassie Blue. It is seen that the angular momentum about the contact point has the advantages discussed above.

### III. LINEAR INVERTED PENDULUM MODEL

This section provides the ubiquitous Linear Inverted Pendulum (LIP) model of Kajita et al. [19]. The LIP model assumes the center of mass moves in a plane, the angular momentum about the center of mass is constant, and the legs are massless. Here, we will express the model in terms of its original coordinates, namely position and linear velocity of the center of mass, and in terms of the proposed new coordinates, namely position and angular momentum about the contact point. The dynamics of the inverted pendulum are exactly linear. Moreover, the 3D dynamics in the  $x$  and  $y$  directions are decoupled, and hence we only need to consider a 2D pendulum.

Let  $H$  denote the height of the center of mass. For a 2D model, the dynamics in the  $x$  direction is

$$\begin{bmatrix} \dot{x} \\ \ddot{x} \end{bmatrix} = \begin{bmatrix} 0 & 1 \\ g/H & 0 \end{bmatrix} \begin{bmatrix} x \\ \dot{x} \end{bmatrix}, \quad (5)$$

where  $x$  is the position of CoM in the frame of contact point. if we assume there is no ankle torque. The solution of this linear system is

$$\begin{bmatrix} x(T) \\ \dot{x}(T) \end{bmatrix} = \begin{bmatrix} \cosh(\ell(T-t)) & 1/\ell \sinh(\ell(T-t)) \\ \ell \sinh(\ell(T-t)) & \cosh(\ell(T-t)) \end{bmatrix} \begin{bmatrix} x(t) \\ \dot{x}(t) \end{bmatrix}, \quad (6)$$

where  $\ell = \sqrt{g/H}$ ,  $t$  is the current time and  $T$  is the (predicted) time of the end of the step.

We assume the body is a point mass and is moving on a horizontal plane, that is the height of the center of mass is constant. Because we are assuming a point mass, the angular

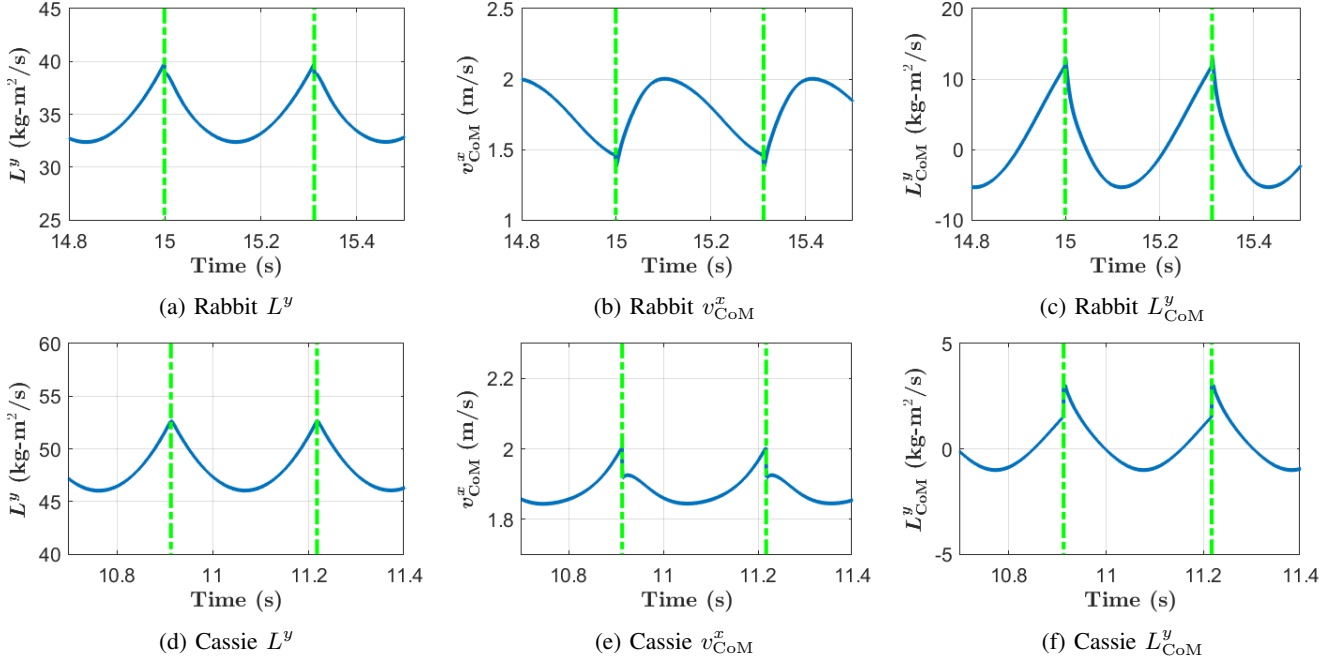


Fig. 4: Comparison of  $L$ ,  $L_{CoM}$ ,  $v_{CoM}^x$  in simulation for the bipedal robots Rabbit and Cassie, while  $v_{CoM}^z$  is carefully regulated to zero. The angular momentum about the contact point,  $L$ , has a convex trajectory, both of which are similar to the trajectory of a LIP model, while the trajectory of the longitudinal velocity of the center of mass,  $v_{CoM}^x$ , has no particular shape. In this figure,  $L$  is continuous at impact, which is based on two conditions:  $v_{CoM}^z = 0$  at impact and the ground is level. Even when these two conditions are not met, the jump in  $L$  at impact can be easily calculated with (3).

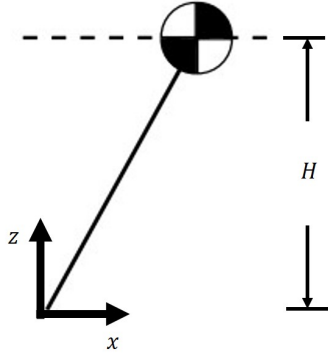


Fig. 5: Linear Inverted Pendulum Model. A prismatic joint in the leg allows the CoM to move along a given line. In the original paper [19], the model requires massless legs, constant  $L_{CoM}$ , and the center of mass moving along a straight (not necessarily horizontal) line. Here, we assume in addition a point mass and a horizontal trajectory for the center of mass.

momentum about the center of mass is zero. We now replace the states  $\{x, \dot{x}\}$  with  $\{x, L^y\}$ , where  $L^y$  is the y-component of angular momentum about the contact point. The corresponding dynamic model is

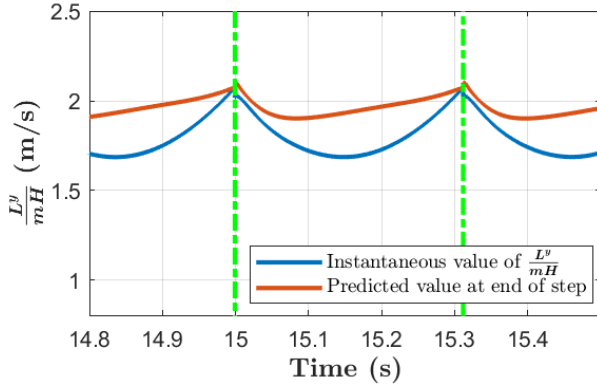
$$\begin{bmatrix} \dot{x} \\ \dot{L}^y \end{bmatrix} = \begin{bmatrix} 0 & 1/mH \\ mg & 0 \end{bmatrix} \begin{bmatrix} x \\ L^y \end{bmatrix}, \quad (7)$$

and its corresponding solution is

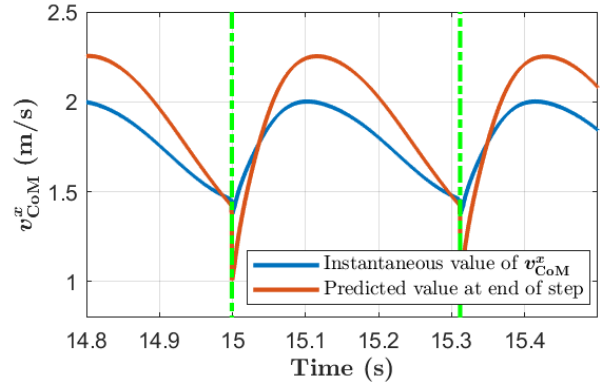
$$\begin{bmatrix} x(T) \\ L^y(T) \end{bmatrix} = \begin{bmatrix} \cosh(\ell(T-t)) & 1/mH\ell \sinh(\ell(T-t)) \\ mH\ell \sinh(\ell(T-t)) & \cosh(\ell(T-t)) \end{bmatrix} \begin{bmatrix} x(t) \\ L^y(t) \end{bmatrix}, \quad (8)$$

where  $t$  is the current time and  $T$  is the (predicted) time of the end of the step.

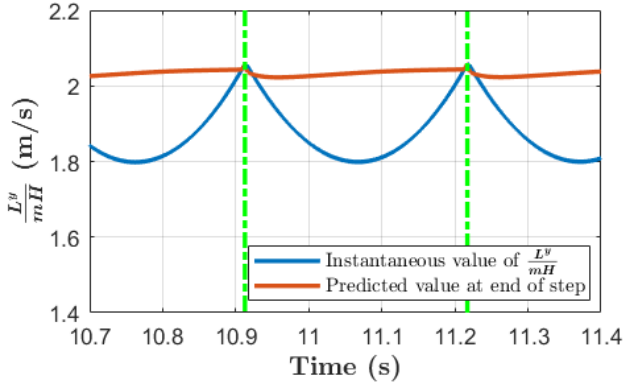
For a point-mass inverted pendulum, where the mass moves on a horizontal plane, representations (5) and (7) are exactly the same. **So what have we gained? Importantly, for a real robot, where the two representations are only approximate, the second one is better for making predictions on the robot's state**, as we discussed in Sec. II. Figure 6 compares the predictions of linear velocity and angular velocity about the contact point for a seven degree of freedom 2D model of Rabbit and a 20 degree of freedom 3D model of Cassie. In the figure, the simulated instantaneous values of  $v_{CoM}^x(t)$  and  $L^y(t)$  are shown in blue. The red line shows the evolution of the predicted values at the end of a step for  $v_{CoM}^x(t)$  and  $L^y(t)$  from (6) and (8) plotted against the corresponding instantaneous values. In a perfect predictor, the predicted values would be straight lines. It is clear that, when extrapolated to a realistic model of a robot, the prediction of angular momentum about the contact point is significantly more reliable than the estimate of linear velocity.



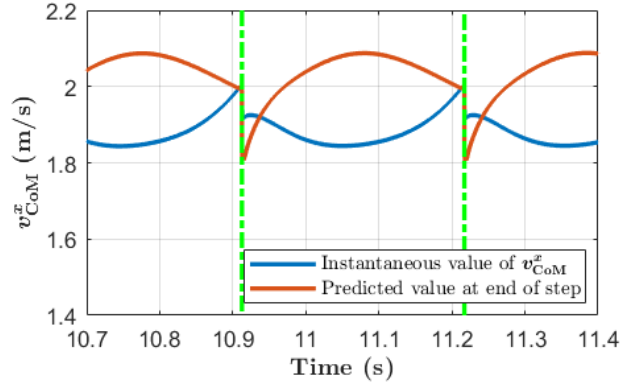
(a) Rabbit  $L^y$  prediction



(b) Rabbit  $v_{CoM}^x$  prediction



(c) Cassie  $L^y$  prediction



(d) Cassie  $v_{CoM}^x$  prediction

Fig. 6: Comparison of the ability to predict velocity vs angular momentum at the end of a step. The most crucial decision in the control of a bipedal robot is where to place the next foot fall. In the standard LIP controller, the decision is based on predicting the longitudinal velocity of the center of mass. In Sect. III we use angular momentum about the contact point. We do this because on realistic bipeds, the LIP model provides a more accurate and reliable prediction of  $L$  than  $v_{CoM}$ . The comparison is more significant on Rabbit, whose leg center of mass is further away from the overall CoM.

#### IV. HIGH-LEVEL CONTROL STRATEGY IN TERMS OF ANGULAR MOMENTUM

Our overall control objective will be to regulate walking speed. Because of the four advantages of angular momentum versus linear velocity that we listed in Sect. III, we will use angular momentum about the contact point as a primary control variable. In this section, we explain our method for deciding where to end one step by initiating contact between the ground and the swing foot, thereby beginning the next step. In robot locomotion control, this is typically called “foot placement control”.

##### A. Notation

We need to distinguish among the following time instances when specifying the control variables.

- $T$  is the step time.
- $T_k$  is the time of the  $k$ th impact.
- $T_k^-$  is the end time of step  $k$ , so that
- $T_k^+$  is the beginning time of step  $k+1$  and  $T_{k+1}^-$  is the end time of step  $k+1$ .

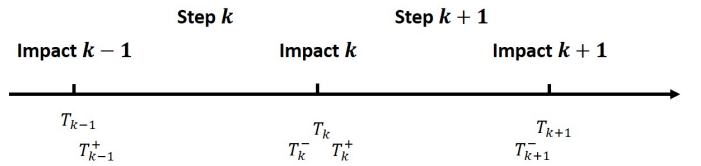


Fig. 7: Definition of  $T_k$

- $(T_k^- - t)$  is the time until the end of step  $k$ .

The superscripts  $+$  and  $-$  on  $T_k$  are due to the impact map; see [30].

- $p_{st \rightarrow CoM}$ . Vector emanating from stance foot to CoM. Here, the stance foot can be thought of as the current contact point.
- $p_{sw \rightarrow CoM}$ . Vector emanating from swing foot to CoM. Here, the swing foot is defining the of contact for the next impact and hence will be a control variable.



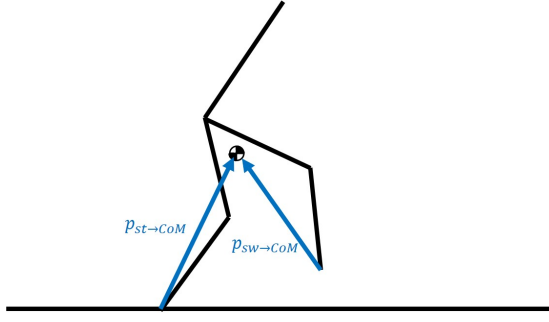


Fig. 8: Definition of  $p_{st \rightarrow CoM}$  and  $p_{sw \rightarrow CoM}$

### B. Foot placement in longitudinal direction

There are multiple means to stabilize gaits [30]. Because we seek to focus on the benefits of using angular momentum instead of linear velocity, the controller we give here simply uses “foot placement” as is commonly associated with the LIP model. **The principal idea is to regulate the angular momentum at the end of the next step by choosing the foot placement position for the end of the current step.**

The Angular Momentum at the end of the next step is related to the Angular Momentum and the position of the center of mass at the beginning of next step by

$$L^y(T_{k+1}^-) = mH\ell \sinh(\ell T) p_{st \rightarrow CoM}^x(T_k^+) + \cosh(\ell T) L^y(T_k^+). \quad (9)$$

However, the CoM position with respect to the stance foot at the beginning of the next step is the same as the CoM position with respect to the swing foot at the end of the current step,

$$p_{st \rightarrow CoM}^x(T_k^+) = p_{sw \rightarrow CoM}^x(T_k^-). \quad (10)$$

Because  $p_{sw \rightarrow CoM}^x(T_k^-)$  is what we can control in the current step, we are motivated to re-write (9) as

$$L^y(T_{k+1}^-) = mH\ell * \sinh(\ell T) p_{sw \rightarrow CoM}^x(T_k^-) + \cosh(\ell T) L^y(T_k^+). \quad (11)$$

Solving (11) for the desired foot position would not yield a causal formula. However, because the CoM height is assumed constant and the ground is flat, the angular momentum about the next contact point is equal to the angular momentum about the current stance leg,

$$L^y(T_k^+) = L^y(T_k^-); \quad (12)$$

see (3). This yields

$$L^y(T_{k+1}^-) = mH\ell \sinh(\ell T) p_{sw \rightarrow CoM}^x(T_k^-) + \cosh(\ell T) L^y(T_k^-). \quad (13)$$

Now, we are almost there. From the second row of (8), an estimate for the angular momentum about the contact point at the end of current step,  $\hat{L}^y(T_k^-)$ , can be continuously estimated by

$$\hat{L}^y(T_k^-)(t) = mH\ell \sinh(\ell(T_k^- - t)) p_{st}^x(t) + \cosh(\ell(T_k^- - t)) L^y(t). \quad (14)$$

If  $L^y(T_{k+1}^-)$  is replaced by its desired value,  $L^{y \text{ des}}(T_{k+1}^-)$ , we now have a causal and implementable expression for desired foot placement,

$$p_{sw \rightarrow CoM}^x(T_k^-)(t) := \frac{L^{y \text{ des}}(T_{k+1}^-) - \cosh(\ell T) \hat{L}^y(T_k^-)(t)}{mH\ell \sinh(\ell T)}. \quad (15)$$

With a perfect estimator for the angular momentum about that stance leg, such as is possible with an ideal LIP model, the desired foot position would be constant. Here, it varies because in a real robot, our estimate for angular momentum evolves with time.

### C. Lateral Control

From (4), the time evolution of the angular momentum about the contact point is decoupled about the  $x$ - and  $y$ -axes. Therefore, once a desired angular momentum at the end of next step is given, Lateral Control is essentially identical to Longitudinal Control and (15) can be applied equally well in the lateral direction. **The question becomes how to decide on  $L^{x \text{ des}}(T_{k+1}^-)$ .**

For walking in place or walking with zero lateral velocity, it is sufficient to obtain  $L^{x \text{ des}}$  from a periodically oscillating LIP model,

$$L^{x \text{ des}}(T_{k+1}^-) = \pm \frac{1}{2} mHW \frac{\ell \sinh(\ell T)}{1 + \cosh(\ell T)}, \quad (16)$$

where  $W$  is the desired step width. The sign is positive if next stance is left stance and negative if next stance is right stance.

### D. Turning

In each step, we suppose there is an angle  $D_k$  which defines the **forward direction** of that step. When walking in a straight line,  $D_k$  is a constant. When the robot makes turns,  $D_k$  will change step by step,  $\Delta D_k = D_{k+1} - D_k \neq 0$ . The  $L^{x \text{ des}}$  and  $L^{y \text{ des}}$  will then be first decided in their corresponding frame defined by  $D_k$ , then transformed back in the world frame and used to decide foot placement in the world frame.

## V. IMPLEMENTING THE LIP-BASED ANGULAR MOMENTUM CONTROLLER ON A REAL ROBOT

In this section we introduce the control variables for Cassie Blue and generate their reference trajectory. As in [9], we leave the stance toe passive. Consequently, there are nine (9) control variables, listed below from the top of the robot to the end of the swing leg,

$$h_0 = \begin{bmatrix} \text{torso pitch} \\ \text{torso roll} \\ \text{stance hip yaw} \\ \text{swing hip yaw} \\ p_{st \rightarrow CoM}^z \\ p_{sw \rightarrow CoM}^x \\ p_{sw \rightarrow CoM}^y \\ p_{sw \rightarrow CoM}^z \\ \text{swing toe absolute pitch} \end{bmatrix}. \quad (17)$$

For later use, we denote the value of  $h_0$  at the beginning of the current step by  $h_0(T_{k-1}^+)$ . When referring to individual components, we'll use  $h_{03}(T_{k-1}^+)$ , for example.

We first discuss variables that are constant. The reference values for torso pitch, torso roll, and swing toe absolute pitch are constant and zero, while the reference for  $p_{st \rightarrow CoM}^z$ , which sets the height of the CoM with respect to the ground, is constant and equal to  $H$ .

We next introduce a phase variable

$$s := \frac{t - T_{k-1}^+}{T} \quad (18)$$

that will be used to define quantities that vary throughout the step to create “leg pumping” and “leg swinging”. The reference trajectories of  $p_{sw \rightarrow CoM}^x$  and  $p_{sw \rightarrow CoM}^y$  are defined such that:

- at the beginning of a step, their reference value is their actual position;
- the reference value at the end of the step implements the foot placement strategy in (15); and
- in between a half-period cosine curve is used to connect them, which is similar to the trajectory of an ordinary (non-inverted) pendulum.

The reference trajectory of  $p_{sw \rightarrow CoM}^z$  assumes the ground is flat and the control is perfect:

- at mid stance, the height of the foot above the ground is given by  $z_{CL}$ , for the desired vertical clearance.

The reference trajectories for the stance hip and swing hip yaw angles are simple straight lines connecting their initial actual position and their desired final positions. For walking in a straight line, the desired final position is zero. To include turning, the final value has to be adjusted. Suppose that a turn angle of  $\Delta D_k^{\text{des}}$  radians is desired. One half of this value is given to each yaw joint:

- $+\frac{1}{2}\Delta D_k^{\text{des}} \rightarrow$  swing hip yaw; and
- $-\frac{1}{2}\Delta D_k^{\text{des}} \rightarrow$  stance hip yaw

The signs may vary with the convention used on other robots.

The final result for Cassie Blue is

$$h_d(s) := \begin{bmatrix} 0 \\ 0 \\ (1-s)h_{03}(T_{k-1}^+) + s(-\frac{1}{2}(\Delta D_k)) \\ (1-s)h_{04}(T_{k-1}^+) + s(\frac{1}{2}(\Delta D_k)) \\ H \\ \frac{1}{2}[(1+\cos(\pi s))h_{06}(T_{k-1}^+) + (1-\cos(\pi s))p_{st \rightarrow CoM}^x(T_k^-)] \\ \frac{1}{2}[(1+\cos(\pi s))h_{07}(T_{k-1}^+) + (1-\cos(\pi s))p_{st \rightarrow CoM}^y(T_k^-)] \\ 4z_{cl}(s-0.5)^2 + (H - z_{CL}); \\ 0 \end{bmatrix}. \quad (19)$$

When implemented with an Input-Output Linearizing Controller so that  $h_0$  tracks  $h_d$ , the above control policy allows Cassie to move in 3D in simulation. Fig. 9 shows Cassie starts from a walking in place gait and accelerate to a speed of 2.8 m/s.

## VI. MODIFICATIONS FOR PRACTICAL IMPLEMENTATION

This section discusses several issues that prevent the basic controller from being implemented on Cassie Blue. Similar issues may or may not arise on your robot.

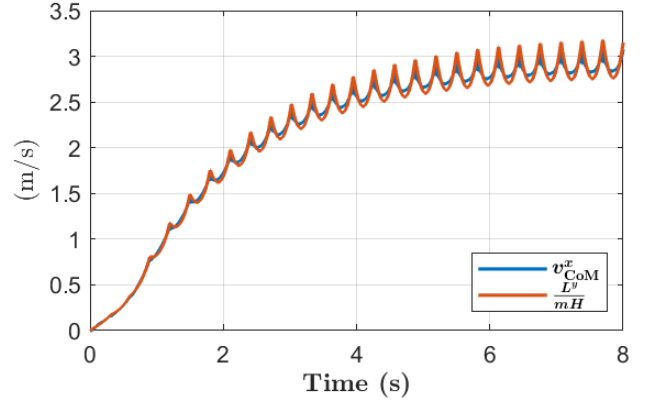


Fig. 9: Simulation results of Cassie.  $\frac{L^x \text{ des}}{mH}$  ramped up from 0 to 3 m/s.

### A. IMU and EKF

In a real robot, an IMU and an EKF are needed to estimate the linear and angular velocities at a fixed point on the robot. Cassie uses a VectorNav IMU. We used the Contact-aided Invariant EKF developed in [14], [15] to estimate the torso velocity. With these signals in hand, we could estimate angular momentum about the contact point.

### B. Filter for Angular Momentum

Angular Momentum about the contact toe could be estimated directly from the sensors on the robot, but it was noisy. We designed a Kalman Filter to improve the estimation. The models we used are

$$\text{Prediction: } L^y(k+1) = L^y(k) + m g p_{st}(k) \Delta T + \delta(k)$$

$$\text{Correction: } L^y(k) = L_{\text{obs}}^y(k) + \epsilon(k) \quad (20)$$

### C. Inverse Kinematics

Input-Output Linearization does not work well in experiments [8], [9], [29]. To use a passivity-based controller for tracking that is inspired by [26], we need to convert the reference trajectories for the variables in (17) to reference trajectories for Cassie’s actuated joints,

$$q^{\text{act}} = \begin{bmatrix} \text{torso pitch} \\ \text{torso roll} \\ \text{stance hip yaw} \\ \text{swing hip yaw} \\ \text{stance knee pitch} \\ \text{swing hip roll} \\ \text{swing hip pitch} \\ \text{swing knee pitch} \\ \text{swing toe pitch} \end{bmatrix}. \quad (21)$$

Iterative inverse kinematics is used to convert the controlled variables in (17) to the actuated joints.

**Why did we not directly use actuated joints?** We used (17) to express the controller objectives because it allows

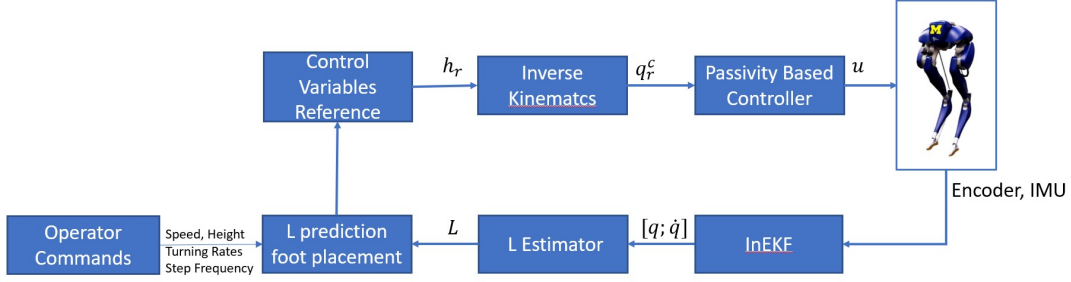


Fig. 10: Block diagram of the implemented controller.

the most intuitive implementation of the basic controller on a physical robot. Also, due to our heritage of using virtual constraints, this is natural to us. Your philosophy may vary.

#### D. Passivity-based Controller

To arrive at a PD controller with feed forward terms, we modified the passivity based controller developed in [26]. The key modifications were:

- transitioning the method to a floating base model of the robot; and
- using the phase variable (18).

This provided improved tracking performance over the straight-up PD implementation in [9].

#### E. Springs

On the swing leg, the spring deflection is small and thus we are able to assume the leg to be rigid. On the stance leg, the spring deflection is not negligible. An offset is added on the knee motor to compensate this spring deflection. While there are encoders to measure the spring deflection, direct use of this leads to oscillations. The deflection of the spring is instead calculated through a simplified model.

#### F. COM Velocity in the Vertical Direction

When Cassie is walking over one meter per second, the assumption that  $v_{\text{CoM}}^z = 0$  breaks down and (12) is no longer valid. Hence, we use

$$L^y(T_k^+) = L^y(T_k^-) + v_{\text{CoM}}^z(T_k^-)(p_{\text{sw} \rightarrow \text{CoM}}^x(T_k^-) - p_{\text{st} \rightarrow \text{CoM}}^x(T_k^-)). \quad (22)$$

From this, the foot placement is updated to

$$p_{\text{sw} \rightarrow \text{CoM}}^{x, \text{des}}(T_k^-) = \frac{L^y \text{des}(T_{k+1}^-) - \frac{(L^y(T_k^-) + mv_{\text{CoM}}^z(T_k^-)p_{\text{st} \rightarrow \text{CoM}}^x(T_k^-)) \cosh(\ell T)}{m(H\ell \sinh(\ell T) - v_{\text{CoM}}^z \cosh(\ell T))}}{m(H\ell \sinh(\ell T) - v_{\text{CoM}}^z \cosh(\ell T))} \quad (23)$$

### VII. EXPERIMENTAL RESULTS

The overall controller summarized in Fig. 10 was implemented on Cassie Blue. The closed-loop system consisting of robot and controller was evaluated in a number of situations that are itemized below.

- **Walking in a straight line on flat ground.** Cassie could walk in place and walk stably for speeds ranging from zero to 2.1 m/s.
- **Diagonal Walking.** Cassie is able to walk simultaneously forward and sideways on grass, at roughly 1 m/s in each direction.
- **Sharp turn.** While walking at roughly 1 m/s, Cassie Blue effected a  $90^\circ$  turn, without slowing down.
- **Rejecting the classical kick to the base of the hips.** Cassie was able to remain upright under “moderate” kicks in the longitudinal direction. The disturbance rejection in the lateral direction is not as robust as the longitudinal, which is mainly caused by Cassie’s physical design: small hip roll motor position limits.
- **Finally we address walking on rough ground.** Cassie Blue was tested on the iconic Wave Field of the University of Michigan North Campus. The foot clearance was increased from 10 cm to 20 cm to handle the highly undulating terrain. Cassie is able to walk through the “valley” between the large humps with ease at a walking pace of roughly 0.75 m/s, without falling in all tests. The row of ridges running east to west in the Wave Field are roughly 60 cm high, with a sinusoidal structure. We estimate the maximum slope to be 40 degrees. Cassie is able to cross several of the large humps in a row, but also fell multiple times. On a more gentle, straight grassy slope of roughly 22 degrees near the laboratory, Cassie can walk up it with no difficulty whatsoever.

### VIII. CONCLUSIONS

We argued that angular momentum about the contact point is a superior variable for planning step placement in a LIP-based controller. We believe the same will hold on many other control strategies. This paper limited itself to a LIP-style controller so that other locomotion groups could clearly assess the benefits of angular momentum about the contact point.

Using our new controller, Cassie was able to accomplish a wide range of tasks with nothing more than common sense task-based tuning: a higher step frequency to walk at 2.1 m/s and extra foot clearance to walk over slopes exceeding 15 degrees. Moreover, in the current implementation, there is no optimization of trajectories used in the implementation on Cassie. The robot’s performance is currently limited by



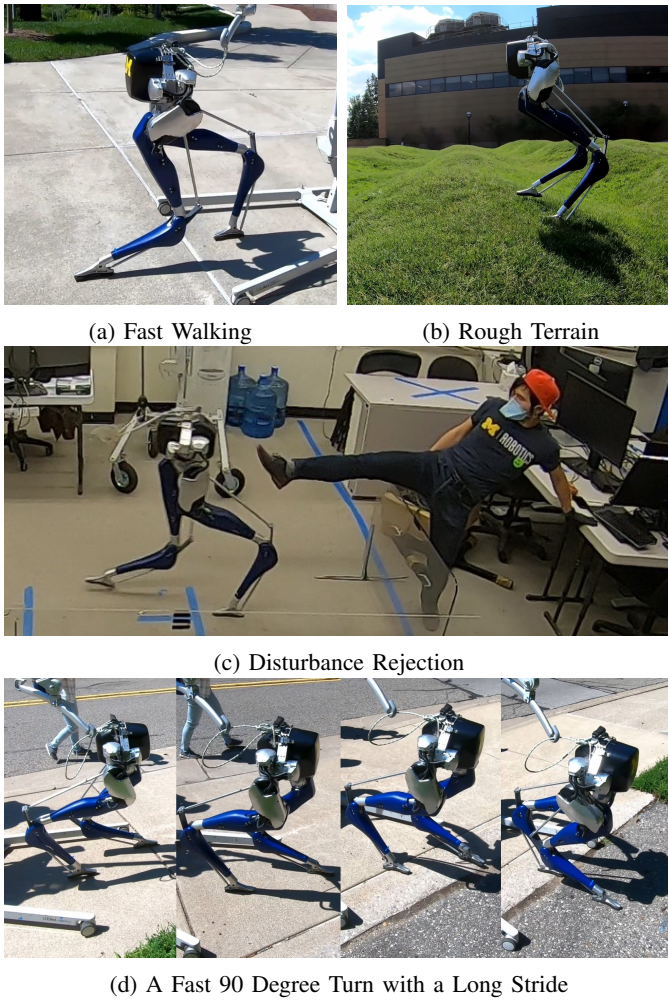


Fig. 11: Images from several closed-loop experiments conducted with Cassie Blue and the controller developed in this paper. Short Footage of those experiments are compiled in video [1]. Longer versions can be found in [2]

the hand-designed trajectories leading to joint-limit violations and foot slippage. These limitations will be alleviated by incorporating optimization.

The current controller tries its best to maintain a zero center of mass velocity in the  $z$ -direction. This simplifies the transition formula for the angular momentum at impact. Our next publication will explain how to exploit changes in the vertical component of the center of mass velocity in order to better achieve a desired angular momentum: foot placement plus  $v_{CoM}^z$ !

## REFERENCES

- [1] Experiment Video Compilation. <https://youtu.be/V36DCsc6iio>.
- [2] Michigan Robotics: Dynamic Legged Locomotion Lab Youtube Channel. <https://www.youtube.com/channel/UCMfDV8rkQqWhUwnTAYaQ0tQ>. Accessed: 2019-01-31.
- [3] R. Blickhan. The spring-mass model for running and hopping. *Journal of Biomechanics*, 22(11-12):1217–1227, 1989.
- [4] C. Chevallereau, G. Abba, Y. Aoustin, F. Plestan, E. R. Westervelt, C. Canudas-de-Wit, and J. W. Grizzle. RABBIT: A testbed for advanced control theory. *IEEE Control Systems Magazine*, 23(5):57–79, October 2003.
- [5] Hongkai Dai and Russ Tedrake. Planning robust walking motion on uneven terrain via convex optimization. In *Humanoid Robots (Humanoids), 2016 IEEE-RAS 16th International Conference on*, pages 579–586. IEEE, 2016.
- [6] M. Dickinson, C. Farley, R. Full, M. Koehel, R. Kram, and S. Lehman. How animals move: An integrative view. *Science*, 288:100–106, April 2000.
- [7] James Freudenberg and Df Looze. Right half plane poles and zeros and design tradeoffs in feedback systems. *IEEE transactions on automatic control*, 30(6):555–565, 1985.
- [8] K. Galloway, K. Sreenath, A. D. Ames, and J. W. Grizzle. Torque saturation in bipedal robotic walking through control lyapunov function-based quadratic programs. *IEEE Access*, 3:323–332, 2015.
- [9] Y. Gong, R. Hartley, X. Da, A. Hereid, O. Harib, J. Huang, and J. Grizzle. Feedback control of a cassie bipedal robot: Walking, standing, and riding a segway. In *2019 American Control Conference (ACC)*, pages 4559–4566, 2019.
- [10] Robert D Gregg, Tommaso Lenzi, Levi J Hargrove, and Jonathon W Sensinger. Virtual constraint control of a powered prosthetic leg: From simulation to experiments with transfemoral amputees. *IEEE Transactions on Robotics*, 2014.
- [11] Brent Griffin and Jessy Grizzle. Nonholonomic virtual constraints and gait optimization for robust walking control. *The International Journal of Robotics Research*, page 0278364917708249, 2016.
- [12] J. W. Grizzle, G. Abba, and F. Plestan. Asymptotically stable walking for biped robots: Analysis via systems with impulse effects. *IEEE Transactions on Automatic Control*, 46(1):51–64, January 2001.
- [13] JW Grizzle, Claude H Moog, and Christine Chevallereau. Nonlinear control of mechanical systems with an unactuated cyclic variable. *IEEE Transactions on Automatic Control*, 50(5):559–576, 2005.
- [14] Ross Hartley. Invariant-EKF. <https://github.com/RossHartley/invariant-ekf>.
- [15] Ross Hartley, Maani Ghaffari, Ryan M Eustice, and Jessy W Grizzle. Contact-aided invariant extended kalman filtering for robot state estimation. *The International Journal of Robotics Research*, 39(4):402–430, 2020.
- [16] Ayonga Hereid, Shishir Kolathaya, and Aaron D Ames. Online hybrid zero dynamics optimal gait generation using legendre pseudospectral optimization. In *To appear in: IEEE Conference on Decision and Control (CDC)*. IEEE, 2016.
- [17] Kazuo Hirai, Masato Hirose, Yuji Haikawa, and Toru Takenaka. The development of honda humanoid robot. In *Robotics and Automation, 1998. Proceedings. 1998 IEEE International Conference on*, volume 2, pages 1321–1326. IEEE, 1998.
- [18] Qiang Huang, Shuuji Kajita, Noriho Koyachi, Kenji Kaneko, Kazuhito Yokoi, Hirohiko Arai, Kiyoshi Komoriya, and Kazuo Tanie. A high stability, smooth walking pattern for a biped robot. In *Robotics and Automation, 1999. Proceedings. 1999 IEEE International Conference on*, volume 1, pages 65–71. IEEE, 1999.
- [19] S. Kajita and K. Tani. Study of dynamic biped locomotion on rugged terrain-derivation and application of the linear inverted pendulum mode. In *Robotics and Automation, 1991. Proceedings., 1991 IEEE International Conference on*, pages 1405–1411 vol.2, 1991.
- [20] Shuuji Kajita, Fumio Kanehiro, Kenji Kaneko, Kiyoshi Fujiwara, Kensuke Harada, Kazuhito Yokoi, and Hirohisa Hirukawa. Biped walking pattern generation by using preview control of zero-moment point. In *ICRA*, volume 3, pages 1620–1626, 2003.
- [21] A. E. Martin, D. C. Post, and J. P. Schmiedeler. The effects of foot geometric properties on the gait of planar bipeds walking under HZD-based control. *The International Journal of Robotics Research*, 33(12):1530–1543, 2014.
- [22] T. A. McMahon and G. C. Cheng. The Mechanics of Running: Hoes does Stiffness Couple with Speed? *Journal of Biomechanics*, 23 (suppl. 1):65–78, 1990.
- [23] J. Pratt and R. Tedrake. Velocity-based stability margins for fast bipedal walking. In Moritz Diehl and Katja Mombaur, editors, *Fast Motions in Biomechanics and Robotics*, volume 340 of *Lecture Notes in Control and Information Sciences*, pages 299–324. Springer Berlin Heidelberg, 2006.

- [24] M. H. Raibert. Hopping in legged systems—modeling and simulation for the two-dimensional one-legged case. *IEEE Transactions on Systems, Man and Cybernetics*, 14(3):451–63, June 1984.
- [25] Jacob P. Reher, Ayonga Hereid, Shishir Kolathaya, Christian M. Hubicki, and Aaron D. Ames. Algorithmic foundations of realizing multi-contact locomotion on the humanoid robot DURUS. In *The International Workshop on the Algorithmic Foundations of Robotics (WAFR)*, 2016.
- [26] Hamid Sadeghian, Christian Ott, Gianluca Garofalo, and Gordon Cheng. Passivity-based control of underactuated biped robots within hybrid zero dynamics approach. In *2017 IEEE International Conference on Robotics and Automation (ICRA)*, pages 4096–4101. IEEE, 2017.
- [27] A. Seyfarth, H. Geyer, M. Gunther, and R. Blickhan. A movement criterion for running. *Journal of Biomechanics*, 35(5):649–55, May 2002.
- [28] Miomir Vukobratovic and Branislav Borovac. Zero-moment point: Thirty five years of its life. *International Journal of Humanoid Robotics*, 01(01):157–173, 2004.
- [29] E. R. Westervelt, G. Buche, and J. W. Grizzle. Experimental validation of a framework for the design of controllers that induce stable walking in planar bipeds. *International Journal of Robotics Research*, 24(6):559–582, June 2004.
- [30] Eric R Westervelt, Christine Chevallereau, Jun Ho Choi, Benjamin Morris, and Jessie W Grizzle. *Feedback control of dynamic bipedal robot locomotion*. CRC press, 2007.